Resonance Assessment of Large-scale Wind Park Connected to Primary Distribution Network

Andrés Argüello, *Member*, *IEEE*, Ricardo Torquato, *Member*, *IEEE*, and Walmir Freitas, *Member*, *IEEE*

***Abstract*—On-shore wind parks are typically connected to the high-voltage (HV) transmission system through a bulk transformer. However, wind generators may be connected directly at a medium-voltage (MV) level, such as a utility-owned primary distribution network, if the network is capable of sustaining the power flow and ensuring adequate power quality for its users. This paper presents the findings of a comprehensive study on the management of resonance in a utility-owned wind park in Costa Rica. The wind park is connected directly to the MV primary distribution network and has no shunt capacitor for power factor correction. The results demonstrate that such configuration has a higher immunity to resonances, as the total grid equivalent impedance perceived by the wind park is typically dominated by the absent HV/MV transformer and shunt capacitor bank. Moreover, the capacitance provided by the underground feeders of the wind park did not result in natural oscillation frequencies in the range of typical harmonic distortions observed in MV distribution networks that violated power quality standards.**

***Index Terms*—Impedance, power distribution, resonance assessment, wind power generation, medium-voltage level.**

I. Introduction

WIND power generation has become one of the most popular alternatives on a worldwide scale to traditional fossil fuel based generation [1]. With the increasing participation of these new technologies at both transmission and distribution levels, utilities have become more aware of the associated technical challenges, such as the robust planning to account for the intermittency of renewable energy resources, and the reduction of overall system inertia [2]. In addition to other challenges associated with the case of distributed energy resources, utilities are obliged to adhere to power quality standards in order to guarantee an adequate voltage supply to their customers. Consequently, there is a need to manage the new potential resonances that may arise from the capacitances introduced by underground cables, filters, and capacitor banks, as well as the negative damping observed in certain bandwidths of wind power generation projects.

From the stability [3]-[5] and the harmonic distortion [6]-[8] perspective, there have been significant advances in recent years in the analysis of resonance phenomena in wind generators. The majority of studies have been conducted on large-scale wind parks, which are fed by dedicated medium-voltage (MV) feeders and connected to the high-voltage (HV) transmission system by bulk transformers. Some of these projects employ series capacitors to compensate for the impedance of long transmission lines and improve their power transfer capability, or shunt capacitors for local reactive power support and power factor correction. However, there are instances in which utilities interconnect wind generators directly with the existing MV primary distribution network without a bulk HV/MV transformer or any type of external capacitive compensation.

From a frequency domain perspective, the absence of transformer and capacitor banks has a significant impact on the driving point impedance of the system, which describes its natural oscillation frequencies. It is therefore of interest to examine the characteristics of the resonances that arise from wind power generation projects connected to MV primary distribution networks.

The harmonic resonance and instability are frequently identified as significant challenges in the literature. This paper presents the results of a comprehensive study conducted on a real Type III wind park in Costa Rica. The park is connected directly to the primary distribution network, which has a lower short-circuit capacity than transmission systems. Additionally, the park does not have a main transformer nor a shunt capacitor bank. This latter point is noteworthy as it is a common topology in Costa Rica and has not been reviewed in the literature. Under practical field conditions, this topology has been observed to exhibit significantly lower risk of problematic resonances, i. e., a higher immunity of this topology to harmonic resonance and greater stability in control-to-grid interactions, compared with the typical topology employed for on-shore large-scale projects connected to the transmission system via bulk transformers. It is anticipated that the findings of this study will inform the develop-

Manuscript received: February 1, 2024; revised: June 11, 2024; accepted: August 9, 2024. Date of CrossCheck: August 9, 2024. Date of online publication: September 2, 2024.

This work was supported in part by TotalEnergies EP Brasil through the ANP regulatory incentive for R&DI and in part by the National Council for Scientific and Technological Development under Grant #306921/2019-7.

A. Argüello (corresponding author) is with the School of Electrical Engineering, University of Costa Rica, San José, Costa Rica (e-mail: andres. arguello. cr@ieee.org).

R. Torquato is with ERA Energy Research and Analytics, Campinas, Brazil (e-mail: torquato@ieee.org).

W. Freitas is with the School of Electrical Engineering and Computation, State University of Campinas, Sao Paulo, Brazil (e-mail: walmir@ieee.org).

DOI: 10.35833/MPCE.2024.000127

ment of electric power quality policy in Costa Rica.

The studies were done with impedance equivalents as they are scalable, precise, and less computationally intensive than the time-domain simulation alternative. Harmonic modal analysis [9] was used to detect the location and frequency of resonances, the conditions to avoid equipment overload due to harmonic resonance [8], as well as the conditions to avoid violations of power quality standards at the point of common connection (PCC) with the grid [7]. Furthermore, the potential for unstable resonances was also discussed.

The rest of this paper is organized as follows. Section II presents a technical comparison between wind parks connected to distribution systems and those connected to transmission systems. Section III presents the modeling approach to studying resonance in a wind park connected to the primary distribution network. Section IV presents a brief discussion on the natural oscillations and stability at resonance, and Section V presents the results of the harmonic resonance analysis due to forced oscillations, as it is the more concerning problem for this specific wind park. The paper is concluded in Section VI.

II. Technical Comparison Between Wind Parks Connected to Distribution Systems and Those Connected to Transmission Systems

A. Concern with Resonance

Modern generators such as Type III and Type IV wind generators feature power electronics converter bridges and controllers acting at multiple bandwidths. The switching of the converters has the potential to generate undesirable harmonic currents. Furthermore, the controllers can be configured to provide negative damping at certain frequencies, which may have implications for the stability of the generators. Simultaneously, wind parks have circuits with capacitances (although modern wind parks typically do not require capacitor banks for reactive compensation) due to the inclusion of filters and underground feeders, which contribute a notable capacitive component. Each capacitance in the circuit, in conjunction with the equivalent inductance observed at its terminals, is associated with a natural oscillation frequency.

If the natural oscillation frequencies of the system match the harmonic distortions present in the grid, or those injected by the generators, they can result in the phenomenon of resonance.

Resonance refers to the amplification of such distortions to higher magnitudes of voltage or current throughout the system, which can lead to undesired protection tripping, abnormal vibrations, and heating, reducing the lifespan of wind park and grid components, and even cause instantaneous damage. Resonances can also result in violations of power quality standards, which could ultimately lead to financial penalties imposed on the wind park operator or the utility by regulatory authorities [10].

B. Relevance of PCC of a Wind Park to Grid

Consider a 64 MVA wind park at different voltage levels, shown in Fig. 1. The grid equivalent in both circuits at the PCC between the wind park and the rest of the grid has a short-circuit capacity of 320 MVA at 60 Hz fundamental frequency and the impedance of the main transformer (Tx) is 15%.

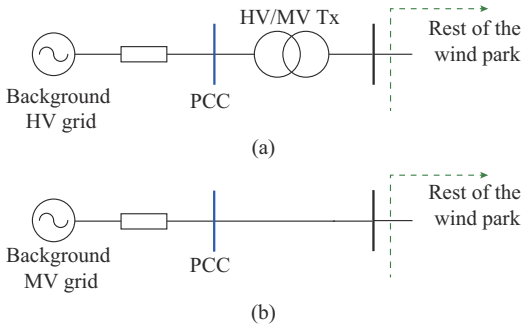

Fig. 1. 64 MVA wind park at different voltage levels. (a) At transmission level. (b) At primary distribution level.

By monitoring the amplification of harmonic distortions from the background grid at PCC resulting from the connection of a wind park to the circuit, it is possible to ascertain the compliance with power quality compatibility standards [10].

The amplification profile of harmonic distortions in the frequency domain can be calculated as a simple voltage divider if we consider the wind park and its generators to be represented by an equivalent impedance [11] and if we further assume that the grid can be modeled by a Thevenin equivalent at the frequencies of study. If the grid distortions have positive sequence, the amplification profile at the PCC of the 64 MVA wind park without capacitor bank at different voltage levels is shown in Fig. 2. The parameters of the wind park that was used are available in [12].

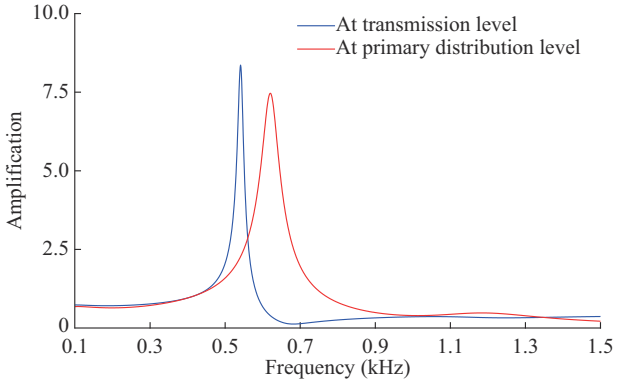

Fig. 2. Amplification profile of positive-sequence harmonic distortions at PCC of 64 MVA wind park without capacitor bank at different voltage levels.

The absence of the HV/MV transformer leads to a considerable difference on the amplification profiles. For example, when the wind park is connected at the transmission level of 230 kV through a bulk transformer, the most visible resonance frequency (which is associated with the filters of the generators) is observed to be approximately 540 Hz. In contrast, when the wind park is connected at the primary distribution level of 34.5 kV, the resonance frequency is observed

to be approximately 620 Hz. Such difference is close to 80 Hz. Overall, the absence of the main transformer causes a shift in the resonances to higher frequencies, resulting from the reduction in inductance within the circuit. The wind park is capable of reaching resonance frequencies with amplification levels above 2, even in the absence of capacitor banks, due to its sufficient capacitance.

As illustrated in Fig. 3, a similar behavior occurs when a shunt capacitor bank is connected at the bus denoting the rest of the wind park in Fig. 1. The presence of this component results in a significant change of the amplification profile when compared with the case without the capacitor bank. The resonance frequency undergoes a shift, moving from 620 Hz to 386 Hz, representing a difference of 234 Hz. Moreover, the amplification level also increases significantly in the case with the capacitor bank.

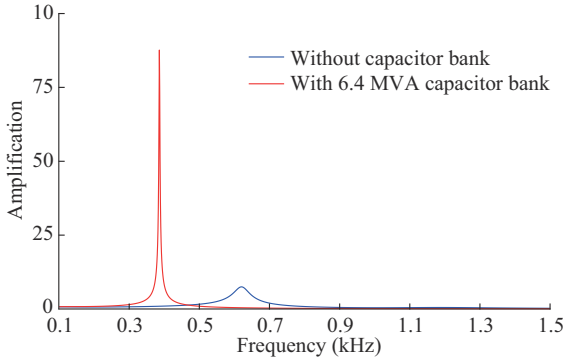

Fig. 3. Amplification profile of positive-sequence harmonic distortions at PCC of 64 MVA wind park connected at primary distribution level.

As most of the existing studies in the literature are based on the topology of wind parks connected to the transmission system or the impact of capacitor banks, this paper presents a case study of a real wind park in Costa Rica connected at the primary distribution level without capacitor banks.

C. Los Santos Wind Park

Coopesantos is a distribution system operator located in the southern region of San José, Costa Rica. Coopesantos owns the sixth wind power generation project that was commissioned in Costa Rica, named Los Santos wind park, which began operating in 2011. It is a complex that has a total capacity of 12.75 MW and comprises 15 wind generators. The aerial view and single-line diagram of the wind park are shown in Fig. 4. It is built with a central overhead feeder and 6 underground feeders, which traverse 7 plots of land (46 hectares) collectively designated as "Fincas" by the utility. Most of the circuit is radial except for Finca 4 that hosts a ring configuration to improve the reliability in case of the outage of a cable section. The energy provided by the wind park covers approximately 30% of Coopesantos customers' total electrical demand.

The 15 wind generators are connected to the MV grid through individual 1 MVA, 34.5 kV/0.69 kV transformers. The generators are of the Siemens Gamesa Type III, G52 model, each with a capacity of 850 kVA at 0.69 kV. The towers stand at a height of 44 m; the blades have a diameter of 44 m; and the generators operate within wind speeds ranging from 4 m/s to 25 m/s, reaching their rated power at 13 m/s. Expression (1) describes the power-wind characteristic, as derived from the data in [13]. Coopesantos reports that the average wind speed v_w at the wind park is 10 m/s, which results in a relatively high capacity factor of 65.8% for a wind power generation project.

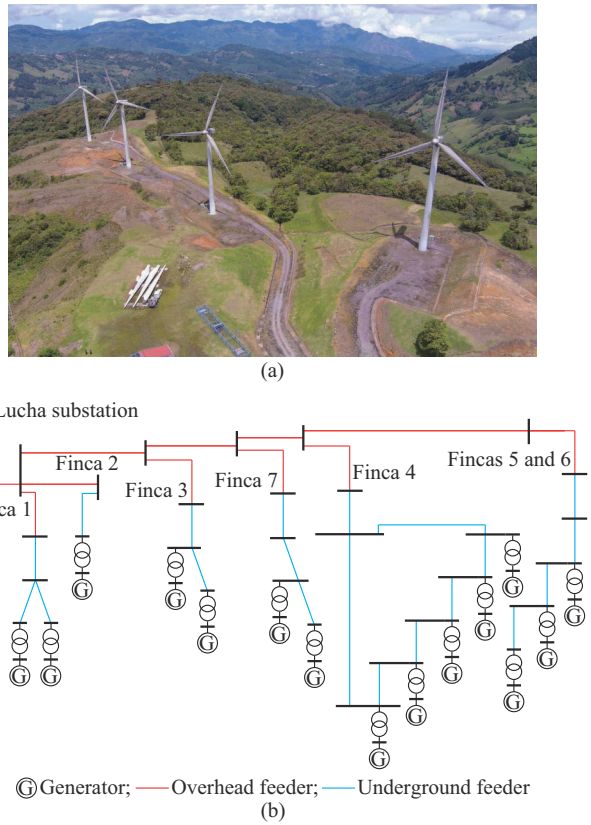

Fig. 4. Aerial view and single-line diagram of Los Santos wind park. (a) Aerial view. (b) Single-line diagram.

$$P = -0.1383v_w^4 + 3.2641v_w^3 - 17.498v_w^2 + 49.78v_w - 69.838 \quad (1)$$

Finally, Los Santos wind park does not use capacitor banks for shunt reactive power compensation, nor it has series capacitor banks for line impedance compensation.

III. Modeling Approach of Resonance

Type III wind generators exhibit a frequency response that depends on their topology and control parameters. Consequently, they are capable of influencing the natural oscillation frequencies of the system [14]. These oscillations have been documented through various events worldwide and can manifest in two distinct ways: as either stable (harmonic resonance, amplification of distortions present in the grid) or unstable (unstable resonance, due to natural system oscillation modes with negative damping introduced by wind generators) [3].

Instead of conducting time-domain simulations with detailed electromagnetic transient models to analyze the resonance phenomenon, it was decided to apply the impedance-based techniques developed in [9] and [12] to analyze the

resonance phenomenon in a simplified and more scalable fashion.

A. Grid Equivalent

The grid equivalent, as observed from the perspective of Los Santos wind park, is situated at the La Lucha substation, as shown in Fig. 4. Coopesantos indicated that the three-phase short-circuit current is $I_{SC,3ph}=1826$ A. If the rated voltage at this point is $V_{MV}=34.5$ kV, the three-phase short-circuit capacity is approximately $S_{SC,3ph}=109.11$ MVA, as calculated with (2). It is important to highlight that such equivalent incorporates the transmission system, the substation equipment, and the rest of the distribution system connected to the secondary of La Lucha substation, which collectively constitute the load.

$$S_{SC,3ph}=\sqrt{3}\,V_{MV}I_{SC,3ph} \tag{2}$$

The grid equivalent is modeled in frequency domain as a voltage source in series with an RL branch. To calculate parameters of the RL branch, it is normally assumed that the impedance of the equivalent circuit is predominantly inductive, so a ratio $X/R=50$ is selected, and the resistance and inductance can be calculated using (3)-(5). *SCR* is the short-circuit ratio with respect to the rated capacity of the wind park $S_{WP}=12.75$ MVA, and the fundamental frequency $f_1=60$ Hz or $\omega_1=2\pi f_1=377$ rad/s. For this circuit, $SCR=8.56$, so that the resistance $R_{SC}=0.2181$ Ω and the inductance $L_{SC}=28.9294$ mH.

$$SCR=S_{SC,3ph}/S_{WP} \tag{3}$$

$$L_{SC}=\frac{V_{MV}^2}{\omega_1 S_{WP}\cdot SCR\cdot\sqrt{1+(X/R)^{-2}}} \tag{4}$$

$$R_{SC}=\omega_1 L_{SC}/(X/R) \tag{5}$$

For a conservative harmonic distortion scenario at La Lucha substation, the harmonic voltages are set to the spectrum in Table I, containing the most common harmonic frequencies in MV and HV systems, where f is the frequency, h is the corresponding harmonic, and V_h is the voltage magnitude of the harmonic. Only the fundamental frequency and the 5th, 7th, 11th, and 13th harmonics are used. The 1th, 7th, and 13th harmonics have positive sequence, whereas the 5th and 11th harmonics have negative sequence.

TABLE I
GRID EQUIVALENT SPECTRUM OF VOLTAGE (BASIS OF 34.5 kV AND 60 HZ)

f (Hz)	h	V_h (p.u.)
60	1	1.00
∈ {300, 420, 660, 780}	∈ {5, 7, 11, 13}	0.03
∉ {60, 300, 420, 660, 780}	∉ {1, 5, 7, 11, 13}	0

The maximum allowable voltage magnitude for individual harmonics in systems with a voltage exceeding 1 kV to 69 kV is 0.03 according to the IEEE Standard 519-2014 [10] and the Costa Rican technical standard AR-NT-SUCAL [15] for monitoring the quality of electric supply in low-voltage (LV) and MV systems. The angles of the harmonic voltages are set to be 0. This allows to model the most conservative operating condition (critical scenario) in the absence of data.

Bus 1 is assigned to the grid equivalent. For harmonic resonance studies, the Thevenin equivalent is transformed into a Norton equivalent, so that the equivalent impedance remains the same, and the current injected into bus 1 is given by:

$$\bar{I}_{h,1}=\frac{\bar{V}_{h,1}}{R_{SC}+\mathrm{j}\omega_1 hL_{SC}} \tag{6}$$

where $\bar{V}_{h,1}$ is the voltage phasor of the h^{th} harmonic at bus 1.

B. Step-up Transformers

The model for 34.5 kV/0.69 kV transformers is a simple RL series branch. The parameters are determined by the short-circuit impedance of the transformer. Skin effect and the parallel branch for magnetization and core iron losses were neglected. According to the data provided by Coopesantos, each wind generator has a 1 MVA transformer, with a short-circuit impedance of $Z_{Tx}=5.5\%$. Assuming the ratio $X/R=50$ for the transformer, similar to the grid equivalent with (4) and (5), the reflected short-circuit resistance of the transformer on the high-voltage side is $R_{Tx}=1.3093$ Ω, and its inductance is $L_{Tx}=173.64$ mH.

The buses for the transformers in the wind park are shown in Table II, where MV bus corresponds to the 34.5 kV winding, and LV bus corresponds to the 0.69 kV winding. The parallel branches for magnetization and iron core losses are not included in this paper, as their effect is not relevant for harmonic frequencies, where they practically become an open circuit.

TABLE II
BUSES FOR TRANSFORMERS IN WIND PARK

MV bus	LV bus	MV bus	LV bus
14	32	24	40
15	33	25	41
16	34	26	42
17	35	27	43
18	36	29	44
20	37	30	45
21	38	31	46
23	39		

C. Feeders

The feeder segments of the wind park were modeled using OpenDSS [16] to incorporate the effect of line geometries into the calculation of per-unit-length resistance, inductance, and capacitance. Such geometries are shown in Fig. 5. Note that the geometry of the overhead feeders is asymmetrical and the lines are not transposed. The phase conductors of the overhead feeders are AAAC 394.5 MCM, while the neutral conductors are AAAC 1/0 AWG. Furthermore, the underground feeder segments are composed of 1/0 AWG 19 STR XLPE copper cables, featuring concentric neutrals and a 15 kV insulation voltage. The resistance, inductance, and capacitance matrices are exported from OpenDSS and are trans-

formed using the Fortescue transform to determine the parameters for positive, negative, and zero sequences.

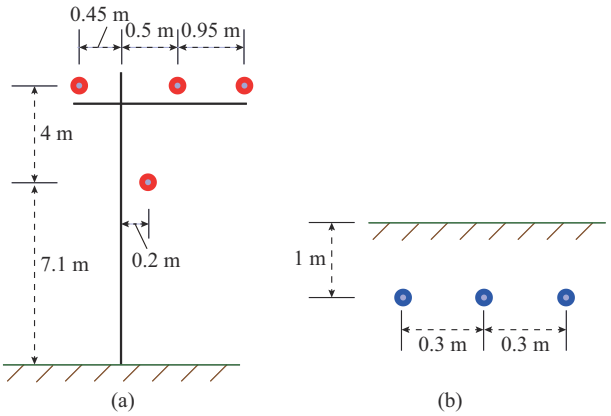

Fig. 5. Line geometries of feeder segments in Los Santos wind park. (a) Overhead feeder. (b) Underground feeder.

Neglecting sequence couplings, it is possible to set the positive- and negative-sequence parameters of the feeders using the data from Table III. S_{max} is the maximum apparent power with the voltage basis of 34.5 kV; and r, l, and c are the per-unit-length resistance, inductance, and capacitance of wind park feeders, respectively. These parameters are used to model the frequency-dependent impedance profile of the feeders, where each segment is modeled with the lumped-parameter pi-line equivalent. The lengths of wind park feeders and the topology is specified in Table IV.

TABLE III
PARAMETERS OF WIND PARK FEEDERS

Feeder type	Ampacity (A)	S_{max} (MVA)	r (Ω/km)	l (mH/km)	c (nF/km)
Overhead	530	32	0.1673	1.0138	11.7376
Underground	230	14	0.4510	0.6704	207.3235

TABLE IV
LENGTHS OF WIND PARK FEEDERS AND TOPOLOGY

Bus i	Bus j	Feeder type	Length (m)	Bus i	Bus j	Feeder type	Length (m)
1	2	Overhead	3623.7	17	18	Underground	105.0
2	3	Overhead	791.1	10	19	Underground	12.0
3	4	Overhead	2540.4	19	20	Underground	96.0
4	5	Overhead	1140.0	20	21	Underground	125.0
5	6	Overhead	1233.3	11	22	Underground	10.0
2	7	Overhead	62.8	22	23	Underground	130.0
2	8	Overhead	44.8	23	24	Underground	360.0
3	9	Overhead	137.3	24	25	Underground	110.0
4	10	Overhead	52.2	25	26	Underground	200.0
5	11	Overhead	270.2	26	27	Underground	330.0
6	12	Overhead	193.1	27	22	Underground	146.0
7	13	Underground	18.0	12	28	Underground	25.0
13	14	Underground	105.0	28	29	Underground	25.0
13	15	Underground	25.0	29	30	Underground	140.0
8	16	Underground	36.0	30	31	Underground	210.0
9	17	Underground	26.0				

D. Generators

The 850 kVA, 0.69 kV Type III wind generators are modeled as a Norton equivalent at varying frequencies, wherein their impedance is contingent upon the topology and control parameters. The literature converges to a typical generator topology and parameter range such as the one in [14]. The model shown in Fig. 6 is used in this paper, with a comprehensive description provided in [12]. In Fig. 6, GSC stands for grid-side converter; and RSC stands for rotor-side converter. Such model is expressed as a descriptor state space form by means of an average converter model and subsequently processed in order to obtain the positive- and negative-sequence impedance profiles at its PCC.

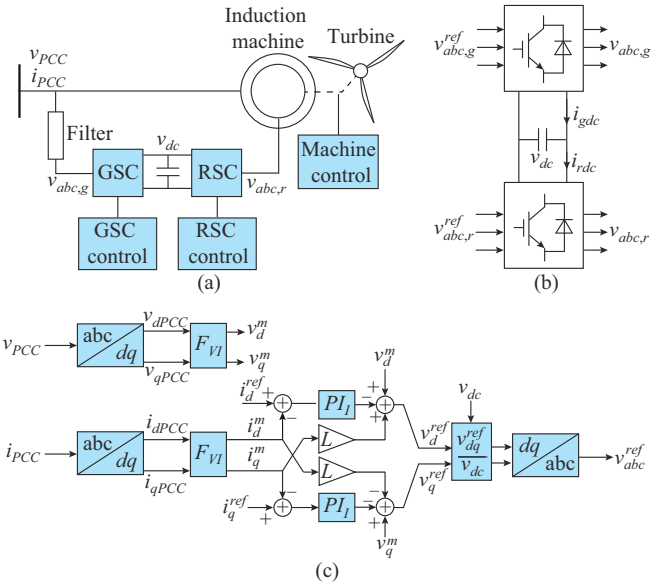

Fig. 6. Summary of Type III wind generator model. (a) Type III wind generator topology. (b) Converter bridge. (c) Converter current control loop.

The impedance profile results for Norton equivalent of Type III wind generator are shown in Fig. 7, where X_{gen} and R_{gen} are the resistance and reactance of the generator impedance, respectively. These profiles were obtained at 10 m/s wind speed and unity power factor, however, these operating point characteristics are primarily significant for the operational setpoint of power electronics at subsynchronous frequencies or frequencies close to the fundamental frequency in weak grids [4], [17].

The next step is to model the current injected by the generators in the Norton equivalent. The consensus in the literature is that modern generators inject negligible harmonic distortions and can be modeled simply as impedances [11]. Reference [18] also mentions that in the presence of grid distortions, the harmonic currents injected by modern generators become negligible. However, due to the absence of measurements and to consider a more conservative scenario, it was decided to include a current distortion profile for the harmonic frequencies obtained from the simulation of the EMT model, as shown in Fig. 8. Finally, the generators are assigned to the LV bus of the transformers, as indicated in Table II. References [19] and [20] can be consulted for further details on the generator modeling.

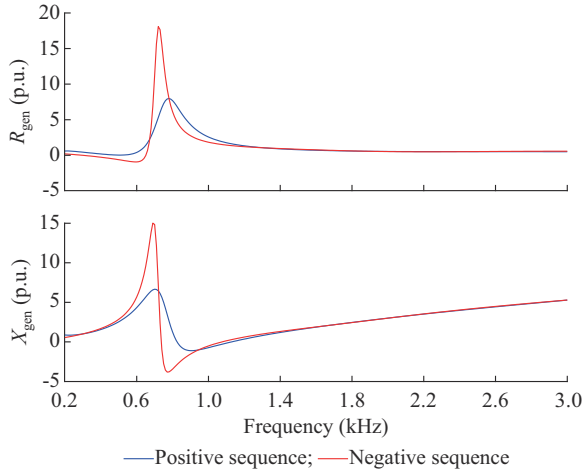

Fig. 7. Impedance profiles for Norton equivalent of Type III wind generator.

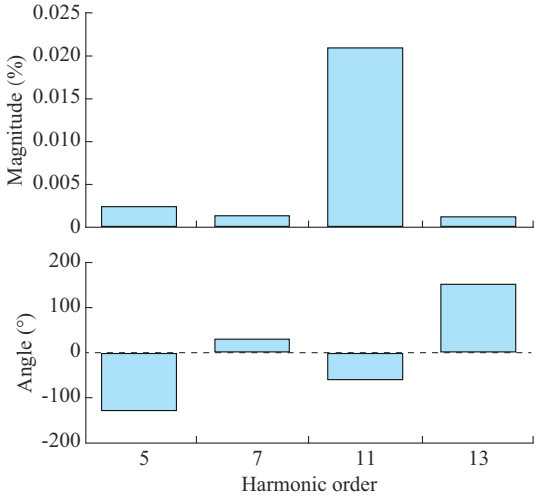

Fig. 8. Harmonic current for Norton equivalent of Type III wind generator.

IV. Natural Oscillations and Stability at Resonance

Even though Los Santos wind park is Type III, it has no series capacitors, so the subsynchronous resonance will not occur [4]. The *SCR* is rather high (about 8 times the capacity of the wind park), so oscillations near the fundamental frequency can also be discarded [21]. Finally, the instability in the harmonic range of frequencies, though unlikely, needs to be assessed.

A. Harmonic Modal Analysis

When the element that defines the resonance is well known, as is the case with capacitor banks, it is more straightforward to conduct a stability analysis by observing the total damping at the natural oscillation frequency. However, in the case of the circuit under study, the capacitive effects are distributed throughout the system in the feeders and generators, as the Los Santos wind park does not have shunt capacitor banks for reactive power compensation.

A useful tool in this case is the harmonic modal analysis, which requires to build the nodal admittance matrix $\boldsymbol{Y}(f)$ of the system at frequency f [9], [22]. The procedure for constructing it is the same as for the regular admittance matrix at the fundamental frequency used in power flow or short-circuit studies. In this paper, the system is modeled with $N=46$ buses, so the nodal admittance matrix in (7) has a dimension of $N\times N$. For each frequency, the impedance of the wind park components is calculated using the models in Section III, and the matrix is updated.

$$\boldsymbol{Y}(f)=\begin{bmatrix} y_{11} & y_{12} & \cdots & y_{1N} \\ y_{21} & y_{22} & \cdots & y_{2N} \\ \vdots & \vdots & & \vdots \\ y_{N1} & y_{N2} & \cdots & y_{NN} \end{bmatrix} \tag{7}$$

The natural oscillation frequencies can be obtained from $\boldsymbol{Y}(f)$, along with the damping ratios, in order to determine the stability of each oscillation mode. This is achieved in a manner analogous to a traditional small disturbance analysis, through the analysis of the state transition matrix of the linearized state space model at fundamental frequency. However, in this instance, the harmonic admittance matrix is considered at frequency f. Similarly, the participation factor can also be calculated in a manner analogous to that described above, which is a metric that allows for the observation of the buses in the system that contribute the most to each mode. Consequently, these factors assist in the identification of the elements responsible for these oscillations.

This harmonic modal analysis differs from the small-signal stability analysis due to the following steps. First, the absolute value of the participation factors is calculated for every f. Then, the minimum value among them is selected, which corresponds to a bus index denoted as c. The eigenvalue corresponding to this subscript c is stored and known as the critical eigenvalue $\lambda_c(f)$ for every f [9]. The process is repeated for the remaining frequencies, and a critical eigenvalue profile is built, as shown in Fig. 9 for Los Santos wind park.

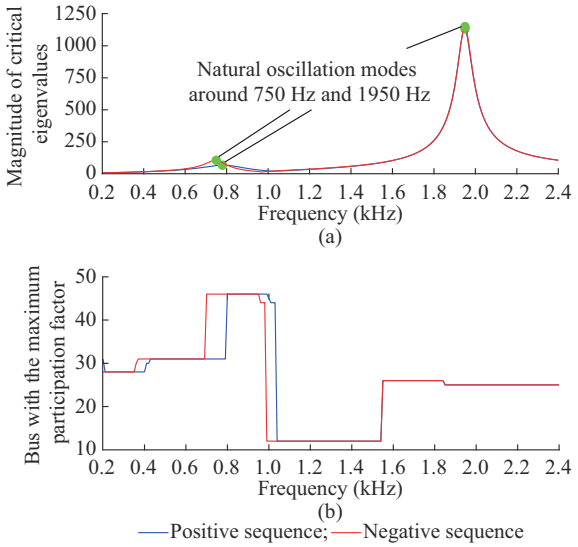

Fig. 9. Critical eigenvalue profile and bus with the maximum participation factor. (a) Critical eigenvalue profile. (b) Bus with the maximum participation factor.

Figure 9(a) shows the magnitude of critical eigenvalues for every frequency that was swept, where the peaks denoted by the green dots correspond to the natural oscillation modes of the system, and Fig. 9(b) shows the bus where the critical eigenvalue was found for each frequency, i.e., the bus where the resonance frequency was located. According to the bus designation from Table II and Table IV, bus 46 and bus 25 indicate that the 750 Hz resonance is associated with the filter of the generators, and the 1950 Hz resonance is associated with the capacitance of the feeders. The damping of the critical eigenvalues that describe the natural oscillation modes of the system at each frequency $\lambda_c(f)=\alpha_c(f)+\mathrm{j}\beta_c(f)$ corresponds to its real part $\alpha_c(f)$. If the damping of the eigenvalue is negative, the system exhibits instability at this frequency with increasing magnitude. If it is 0, the system exhibits a natural oscillation with constant magnitude. If it is positive, the system is stable, and the oscillation is dampened, manifesting only under transient conditions [23].

Two oscillation modes are visible in the interval of harmonic frequencies of Fig. 9. The mode at 750 Hz is located at the generator buses and corresponds to the capacitor of the LCL filter of the generator, while the mode at 1950 Hz is located at the buses of the underground ring of Finca 4, which is attributed to the cable capacitance.

B. Stability at Resonance in Los Santos Wind Park

As vendors typically do not disclose the control and filter topology or parameters of the wind generators, a sensitivity analysis of the following variables was conducted to ascertain whether any circuit configuration could potentially result in unstable resonance in Los Santos wind park.

1) Wind speed

The wind speed is directly linked to the active power injection and the operational setpoint of the generator. This variable was swept from 4 m/s to 13 m/s with a step of 3 m/s.

2) AC voltage/constant reactive power factor control modes

AC voltage control mode and constant reactive power factor control mode (set to unitary) were evaluated.

3) Topologies of front-end filters

The front-end filter of the GSC in the Type III wind generator uses a passive filter to mitigate the high-frequency distortions introduced by the switching of the power electronics converters. The topology of front-end filters is most likely LCL, however, an L topology was also tested.

4) Feed-forward terms of internal current control loop

The internal current control loop of the generators compares the current at converter terminals with the reference value, set by the outer control loops that manage the DC bus voltage and generator power. However, the topology of the feed-forward terms of the generators is commonly unknown, and apart from the typical current feed-forward terms for *dq*-domain decoupling, voltage feed-forward terms can also be included. Both of these terms were tested.

Although the resonance frequencies from the natural oscillation modes denoted by the green dots, as shown in Fig. 10, shifted with the studied variables, the critical eigenvalue profiles remained very similar, and the only study that produced notable difference was the change in the topology of the front-end filter. Only the positive-sequence profiles are shown, as this type of instabilities can be studied as balanced phenomena [12]. The expanded analysis for the front-end filter is shown in Fig. 11, where it is visible that the presence of the capacitor results in a shift in the frequency profile, so that the oscillation modes caused by the feeder capacitors move from approximately 2 kHz to 1.7 kHz. No significant changes were detected at subsynchronous frequencies, which confirms either poor control tunings or series capacitors are required to excite the instability.

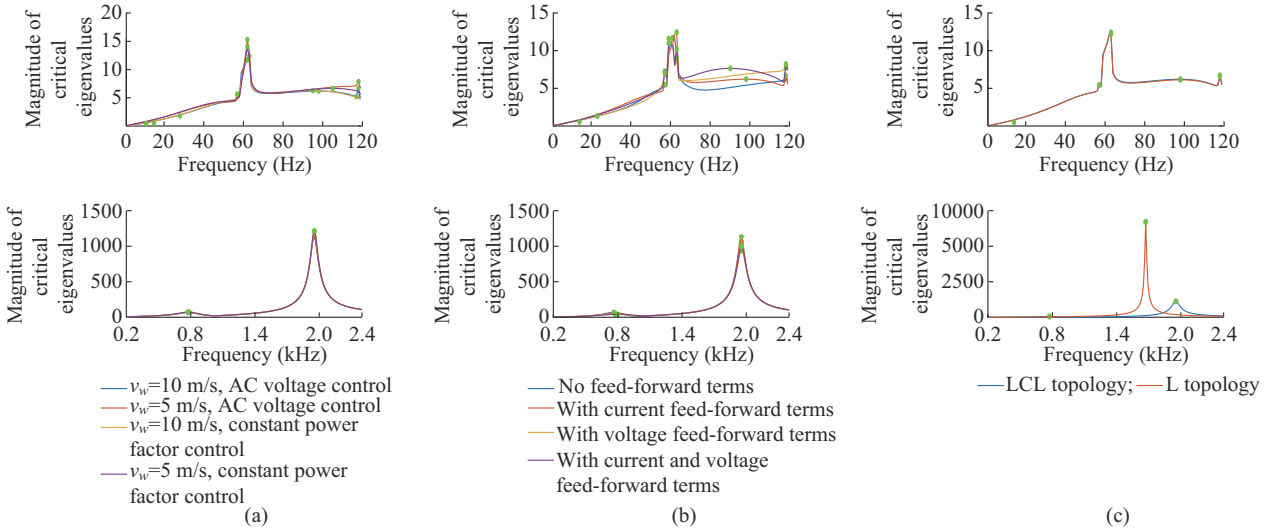

Fig. 10. Sensitivity results of harmonic modal analysis to determine variation in resonance frequency and stability (positive sequence). (a) Wind speed and AC voltage or constant power factor control mode. (b) Feed-forward terms of internal current control loop. (c) Topologies of front-end filters.

Despite the visible presence of oscillation modes in the system across both the low- and high-frequency ranges, all of the tested scenarios were found to be stable. This result corroborates the information provided by Coopesantos, which indicated the absence of documented instances of instability.

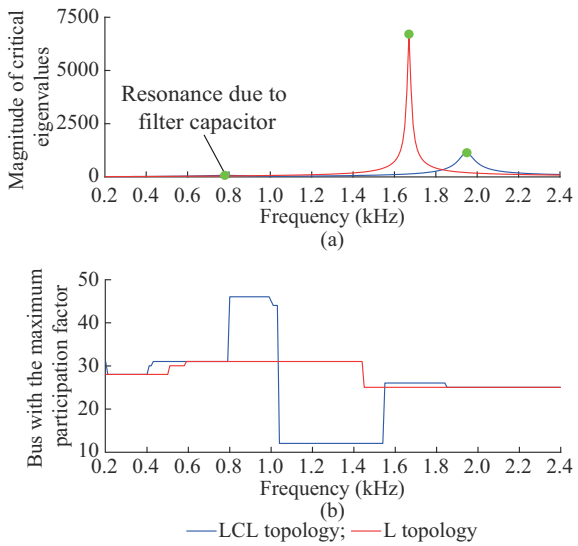

Fig. 11. Profiles of harmonic modal analysis with different topologies of front-end filters (positive sequence).

In conclusion, the results for the present case study of Los Santos wind park indicate that wind power generation facilities connected to the primary distribution network show a better immunity to unstable resonance than wind parks connected to the transmission system. This sensitivity analysis is not meant to be exhaustive, as control parameters such as control delay and proportional-integral (PI) gains are able to play an important role in stability [12].

V. Results of Harmonic Resonance Analysis due to Forced Oscillations

The results of the studies in the previous section indicate that wind parks connected to primary distribution networks have a good immunity to unstable resonances. However, both the grid and the wind generators can act as harmonic distortion sources, which can be magnified if there is positive low damping at a natural oscillation frequency similar to that of the distortion, resulting in the harmonic resonance phenomenon.

In this paper, the effect of harmonic resonance on the system is studied by solving (8) to obtain the bus voltages at the harmonic frequencies, which allow to calculate indices such as the total harmonic distortion of voltage THD_V, the root mean square (RMS) values of voltage V_{rms} and current I_{rms}, the peak voltage V_{peak}, and the apparent power S [8]. Note that $\boldsymbol{Y}(f)$ is the same nodal admittance matrix that was used in the previous stability study. Array of nodal voltage phasors $\bar{\boldsymbol{V}}(f)$ defines the resulting harmonic voltages, whereas array of nodal current phasors $\bar{\boldsymbol{I}}(f)$ models the current injections of the generators at buses 32 to 46 and the Norton equivalent of the grid at bus 1.

$$\bar{\boldsymbol{V}}(f)=\boldsymbol{Y}^{-1}(f)\bar{\boldsymbol{I}}(f) \tag{8}$$

The harmonic voltage distortions of the grid equivalent are set to be the values in Table I, which represent the maximum permissible values for the individual distortions in MV systems in accordance with the Costa Rican technical standard AR-NT-SUCAL [15] that is based on IEEE Standard 519-2014 [10]. Despite the expectation that modern generators will inject negligible harmonic distortions below the switching frequency of their converters [11], [24], the distortion profile in Fig. 8 was considered for all generators. These assumptions were made in the absence of measurement campaigns and thus represent the most conservative condition. Therefore, if the wind park is able to operate without issues under such conditions, the utility should not worry about problematic harmonic resonance issues in the near future. For example, consider the results in Fig. 12 with the magnitude of harmonic voltages at 4 points in the grid (bus 1 at the substation, bus 46 at the farthest generator from the substation in Finca 6, bus 4 at the center of the overhead feeders in Finca 7, and bus 25 in the middle of the underground ring of Finca 4). The voltage magnitude corresponding to the 11th harmonic is the highest due to the presence of a nearby resonance at 750 Hz, as shown in Fig. 9 (harmonic order of 12.5). However, none of the voltage magnitudes exceed the maximum value of 0.03 (dashed red line in Fig. 12), so the wind park appears to provide sufficient damping at the harmonic frequencies.

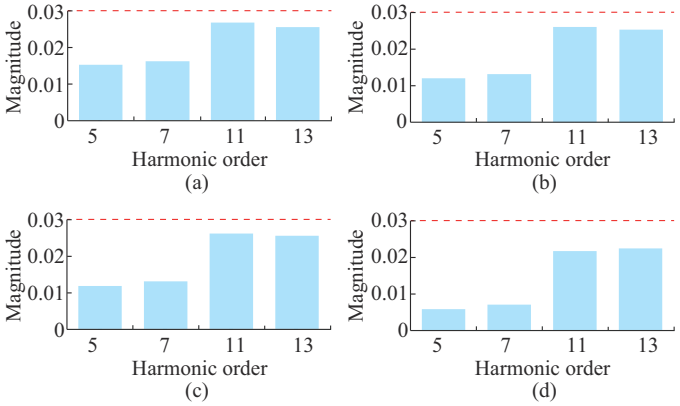

Fig. 12. Magnitudes of harmonic voltages at different points in grid. (a) Bus 1. (b) Bus 25. (a) Bus 4. (a) Bus 46.

A. Compliance with the Maximum Harmonic Distortion Levels

This subsection devotes to the calculation of THD_V, which is of particular relevance at the PCC between the wind park and the grid. This is because it is at this point that regulatory authorities verify for compliance with the power quality standard. THD_V at any bus is calculated with (9), where V is the magnitude of the harmonic voltage. The maximum THD_V according to Costa Rican standard AR-NT-SUCAL is 5% in MV systems with a voltage exceeding 1 kV to 69 kV [15].

$$THD_V=100\sqrt{V^2(5)+V^2(7)+V^2(11)+V^2(13)} \tag{9}$$

Considering the results from Fig. 12, bus 1 has a THD_V of 4.49%, bus 4 has a THD_V of 4.29%, bus 25 has a THD_V of 4.28%, and bus 46 has a THD_V of 3.54%. All of these values are below the allowed distortion limit.

To demonstrate that the wind conditions do not alter the distortion levels significantly across the wind park, Fig. 13 presents a sensitivity analysis of THD_V for all buses in wind

park in terms of wind speed. It is notable that no significant change is observed.

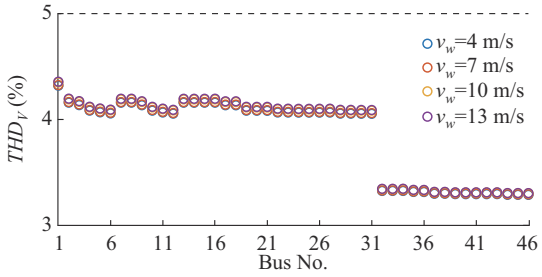

Fig. 13. Sensitivity analysis of THD_V for all buses in wind park in terms of wind speed.

Additionally, the highest point of distortion occurs at the PCC (bus 1), whereas the lowest ones occur at the generator buses (buses 32-46). This indicates that the filters of generators, in conjunction with the wind park feeder, serve to effectively mitigate grid voltage distortions, which have been identified as the predominant factor over generator current distortions [18]. The mitigation effect can be observed in the positive-sequence resistance of the equivalent impedance of wind park at PCC, as shown in Fig. 14, where X_{wp} and R_{wp} are the reactance and resistance of the equivalent impedance of wind park, respectively.

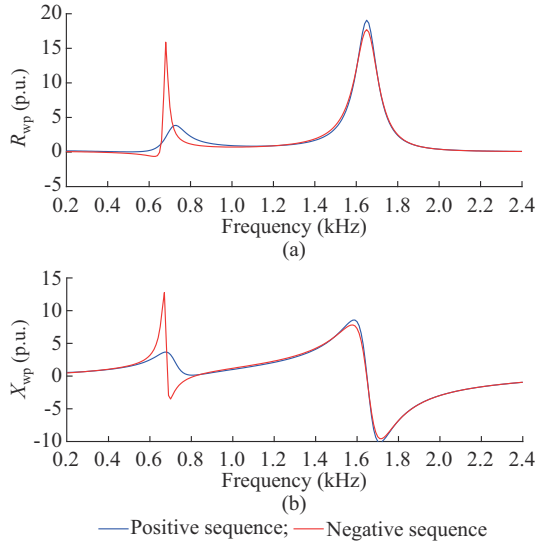

Fig. 14. Equivalent impedance profiles of wind park at PCC.

The most critical variable that influences THD_V is the number of generator outages, as shown in Fig. 15. Note that the less the generators in the grid, the higher the voltage distortion levels in the wind park. This phenomenon can be attributed to the fact that the filters of the generators act as low impedance paths for the grid distortions. Although THD_V in the scenario of 10 generator outages violates the 5% limit, THD_V set for the grid in this study is rather high, so the utility should not be concerned with THD_V violations.

To further understand the harmonic resonance phenomenon in wind parks with the similar topology, Fig. 16 presents a sensitivity analysis of THD_V in the wind park in terms of different multipliers of original feeder lengths. Note that a wind park with twice the original feeder lengths would incur in violation of THD_V at the overhead feeders. However, this is not the case for the generator buses, where the distortions are damped by their transformers and filters.

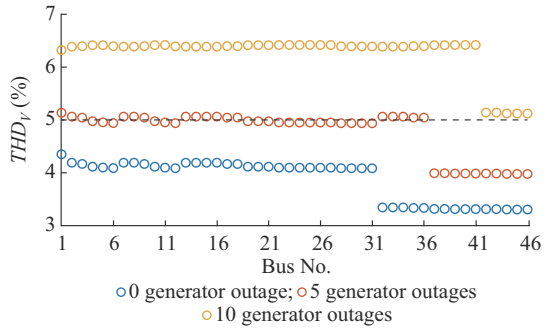

Fig. 15. Sensitivity analysis of THD_V in wind park in terms of different generator outages.

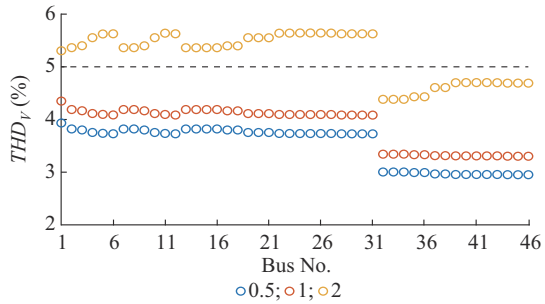

Fig. 16. Sensitivity analysis of THD_V in wind park in terms of different multipliers of original feeder lengths.

Other factors such as controller topologies, gains, and delays, as well as filter topologies and parameters, can also impact the distortion profile in the wind park. It is recommended that the methodology proposed in this paper be reproduced for other wind park circuits that share the characteristics of connection to the primary distribution network, specifically those that do not have main transformer or capacitor bank. This will further allow for the generalization of lower risk of problematic resonances to be explored.

B. Overload of Wind Park Components

Reference [8] presents the equations used to calculate the additional load of wind park components under harmonic distortions. The inputs to the equations are the harmonic voltages from the solution of (8) and the impedance of wind park elements. The loadings of feeders, transformers, and generators in the base case scenario with generators operating at a wind speed of 10 m/s and with voltage regulation at their terminals are shown in Tables V, VI, and VII, respectively. The RMS value of voltage in transformers and feeders is equal to the maximum value observed in the corresponding two buses.

The limits for each performance metric are obtained from international standards and manufacturer datasheets [8]. A summary of typical index limits of different components used for this study is presented in Table VIII.

TABLE V
FEEDER LOADING IN BASE CASE SCENARIO

Bus i	Bus j	V_{rms} (p.u.)	I_{rms} (%)	S (%)	Bus i	Bus j	V_{rms} (p.u.)	I_{rms} (%)	S (%)
1	2	1.0057	26.41	26.53	17	18	1.0083	4.06	4.09
2	3	1.0083	21.11	21.26	10	19	1.0093	8.11	8.17
3	4	1.0092	17.58	17.72	19	20	1.0084	8.11	8.17
4	5	1.0096	14.06	14.18	20	21	1.0094	4.06	4.09
5	6	1.0096	5.27	5.32	11	22	1.0096	20.25	20.42
2	7	1.0057	3.53	3.55	22	23	1.0095	10.25	10.34
2	8	1.0058	1.77	1.77	23	24	1.0096	6.20	6.25
3	9	1.0083	3.53	3.55	24	25	1.0096	2.15	2.17
4	10	1.0093	3.52	3.55	25	26	1.0095	1.90	1.92
5	11	1.0096	8.79	8.86	26	27	1.0096	5.95	6.00
6	12	1.0048	5.27	5.29	27	22	1.0096	10.00	10.08
7	13	1.0049	8.13	8.16	12	28	1.0096	12.15	12.25
13	14	1.0049	4.07	4.08	28	29	1.0097	12.15	12.25
13	15	1.0049	4.07	4.08	29	30	1.0097	8.10	8.17
8	16	1.0058	4.07	4.09	30	31	1.0097	4.05	4.08
9	17	1.0083	8.13	8.18					

TABLE VI
TRANSFORMER LOADING IN BASE CASE SCENARIO

Bus i	Bus j	V_{rms} (p.u.)	I_{rms} (%)	S (%)
14	32	1.0048	56.70	56.91
15	33	1.0048	56.70	56.91
16	34	1.0058	56.70	56.96
17	35	1.0058	56.64	56.90
18	36	1.0083	56.64	57.04
20	37	1.0084	56.47	56.87
21	38	1.0094	56.47	56.93
23	39	1.0095	56.40	56.87
24	40	1.0096	56.39	56.86
25	41	1.0095	56.39	56.86
26	42	1.0094	56.39	56.86
27	43	1.0096	56.40	56.88
29	44	1.0097	56.39	56.86
30	45	1.0097	56.38	56.86
31	46	1.0070	56.38	56.73

It was observed that no components were found to be overloaded in any of the test scenarios, which include varying wind speeds, types of voltage control, and power factor. The transformers (1 MVA, operating at only 0.85 p. u. of their capacity when the generators operate at full capacity) and the feeders are both oversized and possess sufficient capacity to accommodate the additional load imposed by the harmonic frequencies. Additionally, in the previous sections, an absence of problematic harmonic resonances was determined, thereby eliminating the possibility of overloads for the components.

Tests were conducted with the generators operating at full capacity (wind speed of 15 m/s) and with voltage regulation at their terminals, which represents the most critical condition for generator loading. However, since the generators were designed to operate at 110% of their rated power, it was not possible to force them into overload conditions. Overall, it can be affirmed that the Los Santos wind park also has good immunity to harmonic resonance and does not require mitigation measures such as specialized filters.

TABLE VII
GENERATOR LOADING IN BASE CASE SCENARIO

Bus	V_{rms} (p.u.)	I_{rms} (%)	S (%)
32	1.0038	65.78	65.93
33	1.0038	65.78	65.93
34	1.0046	65.78	65.98
35	1.0046	65.73	65.93
36	1.0066	65.72	66.06
37	1.0066	65.58	65.92
38	1.0075	65.58	65.97
39	1.0076	65.52	65.92
40	1.0076	65.52	65.91
41	1.0076	65.51	65.91
42	1.0067	65.52	65.91
43	1.0069	65.52	65.92
44	1.0069	65.51	65.92
45	1.0070	65.51	65.92
46	1.0070	65.50	65.91

TABLE VIII
TYPICAL INDEX LIMITS OF DIFFERENT COMPONENTS

Component	V_{rms} (p.u.)	I_{rms} (%)	S (%)
Generator	1.1	110	110
Feeder	1.2	100	100
Transformer	1.1	105	100

VI. CONCLUSION

This paper presented the results of a case study of resonance assessment in the Los Santos wind park, a wind power generation facility owned by a utility named Coopesantos in Costa Rica.

A model was constructed for the fundamental frequency and in frequency domain, allowing for the calculation of natural oscillation frequencies and system stability. The model was also used to study if distortions present in the grid or introduced by the generators could potentially excite natural oscillation modes (resonances) typically associated with system capacitances.

In contrast to previous work, this study modeled a real wind park with asymmetric overhead and underground feeders, which directly connects to the MV primary distribution network of the utility without a coupling transformer. Furthermore, the harmonic modal analysis was implemented to assess the characteristics of the resonances of the wind park as a whole due to the absence of capacitor banks.

As its key results, no unstable oscillation modes were detected due to the absence of capacitor banks in the vicinity of the wind park and the high short-circuit capacity at the

PCC relative to the wind park size. Simultaneously, the harmonic resonance studies found no violations of voltage distortion limits set by standards or vendor datasheets, and no indications of overloading of wind park components. It is worth noting that the circuit topology under study has a better immunity than the traditional wind park topologies connected to transmission systems. However, more studies can be conducted with other real wind parks to generalize the results. The absence of a shunt capacitor bank does not completely eliminate the risk of problematic harmonic amplification due to the presence of line parasitic capacitance, mainly provided by the underground feeders. It can also be noted that the absence of the main transformer is analogous to connecting the wind park to a stronger grid relative to its rated capacity. Both of these conditions help reduce the risk of problematic harmonic resonances and provide sufficient damping to a prevent instability. It is important to highlight that the aim of this paper is not to generalize the results obtained for this wind park, but rather to give an insight into how the absence of a bulk transformer and a capacitor bank, and the connection of the wind park to a distribution network, help to improve the immunity to resonances. With these results, the utility was able to confirm the adequacy of its power quality and, consequently, to exclude the necessity for potential measures to mitigate distortions or unwanted oscillations.

This study is the first of its kind in Costa Rica, and the methodology is expected to be applied to other existing and future wind and solar parks. This will facilitate the implementation of measurement campaigns prior to and following the commissioning of new projects, thereby providing valuable insights to assess compliance with power quality regulation and code development at MV and HV systems in the national power grid.

REFERENCES

[1] IEA. (2024, Jun.). Renewables 2023: analysis and forecast to 2028. [Online]. Available: https://managenergy. ec. europa. eu/publications/renewables-2023-analysis-and-forecast-2028_en

[2] S. D. Ahmed, F. S. M. Al-Ismail, M. Shafiullah *et al*., "Grid integration challenges of wind energy: a review," *IEEE Access*, vol. 8, pp. 10857-10878, Jan. 2020.

[3] N. Hatziargyriou, J. Milanović, C. Rahmann *et al*. (2020, May). Stability definitions and characterization of dynamic behavior in systems with high penetration of power electronic interfaced technologies. [Online]. Available: https://resourcecenter. ieee-pes. org/publications/technical-reports/pes_tp_tr77_psdp_stability_051320

[4] X. Xie, Y. Zhan, J. Shair *et al*., "Identifying the source of subsynchronous control interaction via wide-area monitoring of sub/super-synchronous power flows," *IEEE Transactions on Power Delivery*, vol. 35, no. 5, pp. 2177-2185, Oct. 2020.

[5] E. Ebrahimzadeh, F. Blaabjerg, X. Wang *et al*., "Harmonic stability and resonance analysis in large PMSG-based wind power plants," *IEEE Transactions on Sustainable Energy*, vol. 9, no. 1, pp. 12-23, Jan. 2018.

[6] Z. Liu, J. Rong, G. Zhao *et al*., "Harmonic assessment for wind parks based on sensitivity analysis," *IEEE Transactions on Sustainable Energy*, vol. 8, no. 4, pp. 1373-1382, Oct. 2017.

[7] R. Torquato, A. Argüello, and W. Freitas, "Comparative analysis between the effect of Type III and Type IV generators on risk of harmonic resonances in wind parks," *IEEE Transactions on Power Delivery*, vol. 38, no. 2, pp. 1169-1181, Apr. 2023.

[8] A. Arguello, R. Torquato, W. Freitas *et al*., "A graphical method to assess component overload due to harmonic resonances in wind parks," in *Proceedings of 2022 IEEE PES General Meeting*, Denver, USA, Jun. 2022, pp. 1819-1828.

[9] W. Xu, Z. Huang, Y. Cui *et al*., "Harmonic resonance mode analysis," *IEEE Transactions on Power Delivery*, vol. 20, no. 2, pp. 1182-1190, Apr. 2005.

[11] W. Xu. (2023, Jan.). Interconnection of inverter-based resources - power quality aspects. [Online]. Available: https://resourcecenter. smartgrid. ieee.org/education/webinar-slides/sgslw0185

[12] A. Argüello, "Methodologies for analysis, management and mitigation of resonance in wind parks," Ph. D. dissertation, State University of Campinas, Sao Paulo, Brazil, 2022.

[13] Wind Generator Models. (2023, Jun.). Gamesa G52. [Online]. Available: https://es.wind-generator-models.com/generators/45-gamesa-g52

[14] I. Vieto and J. Sun, "Sequence impedance modeling and analysis of type-III wind generators," *IEEE Transactions on Energy Conversion*, vol. 33, no. 2, pp. 537-545, Jun. 2018.

[15] ARESEP. (2015, Aug.). AR-NT-SUCAL supervision of the low and medium voltage electrical supply quality. [Online]. https://aresep. go. cr/wp-content/ uploads/2015/08/ Norma_ tecnica_ supervision_ de_ la_ calidad _ del_ suministro_ electrico_ en_ baja_ y_ media_ tension_ AR-NT-SUCAL-2015_ actualizada_ a_ febrero_ 2016.pdf

[16] P. Meira. (2024, Jan.). DSS-Extensions. [Online]. Available: https://dss-extensions.org/

[17] H. Liu, X. Xie, J. He *et al*., "Subsynchronous interaction between direct-drive PMSG based wind farms and weak AC networks," *IEEE Transactions on Power Systems*, vol. 32, no. 6, pp. 4708-4720, Nov. 2017.

[18] K. Yang, M. H. J. Bollen, H. Amaris *et al*., "Decompositions of harmonic propagation in wind power plant," *Electric Power Systems Research*, vol. 141, pp. 84-90, Dec. 2016.

[19] C. Larose, R. Gagnon, P. Prud'Homme *et al*., "Type-III wind power plant harmonic emissions: field measurements and aggregation guidelines for adequate representation of harmonics," *IEEE Transactions on Sustainable Energy*, vol. 4, no. 3, pp. 797-804, Jul. 2013.

[20] K. Yang, M. H. J. Bollen, and E. O. A. Larsson, "Aggregation and amplification of wind-generator harmonic emission in a wind park," *IEEE Transactions on Power Delivery*, vol. 30, no. 2, pp. 791-799, Apr. 2015.

[21] A. Argüello, "Setpoint feasibility and stability of wind park control interactions at weak grids," *Journal of Modern Power Systems and Clean Energy*, vol. 10, no. 6, pp. 1790-1796, Nov. 2022.

[22] L. Hong, W. Shu, J. Wang *et al*., "Harmonic resonance investigation of a multi-inverter grid-connected system using resonance modal analysis," *IEEE Transactions on Power Delivery*, vol. 34, no. 1, pp. 63-72, Feb. 2019.

[23] J. Sun, "Impedance-based stability criterion for grid-connected inverters," *IEEE Transactions on Power Electronics*, vol. 26, no. 11, pp. 3075-3078, Nov. 2011.

[24] X. Wang and F. Blaabjerg, "Harmonic stability in power electronic-based power systems: concept, modeling, and analysis," *IEEE Transactions on Smart Grid*, vol. 10, no. 3, pp. 2858-2870, May 2019.

Andrés Argüello received the Ph. D. degree in electrical engineering from the University of Campinas, Sao Paulo, Brazil, in 2022. He is currently an Associate Professor at the University of Costa Rica, San José, Costa Rica. His research interests include power quality and power system stability.

Ricardo Torquato received the Ph. D. degree in electrical engineering from the University of Campinas, Sao Paulo, Brazil, in 2018. He is currently a Consultant at ERA Energy Research and Analytics, Sao Paulo, Brazil. His research interests include power quality, analysis of distribution system, and distributed generation.

Walmir Freitas received the Ph.D. degree in electrical engineering from the University of Campinas, Sao Paulo, Brazil, in 2001. He is currently a Professor at the same university. His research interests include distribution system, distributed generation, and power quality.